Performance of Pressure Routing in Drifting 3D Underwater Sensor Networks for Deep Water Monitoring

Yu Ren Winston K.G. Seah Paul D. Teal
School of Engineering and Computer Science, Victoria University of Wellington
PO Box 600, Wellington, New Zealand
{yu.ren,winston.seah,paul.teal}@ecs.vuw.ac.nz

ABSTRACT

Recent events such as the 2010 *Deepwater Horizon* oil spill have highlighted the need for ocean monitoring along a specific depth horizon. A mobile underwater acoustic sensor network drifting with the pollution pattern and reporting to radio-equipped surface buoys can provide wide coverage, real-time sensing and can be deployed efficiently. This paper investigates the feasibility of such a network application by evaluating the performance of two recent pressure routing protocols: Depth Based Routing and HydroCast for delivering sensed data from a depth-restricted layer of nodes. Previous work on these protocols has only focused on low-traffic scenarios with infrequent broadcasts made by nodes throughout the network, or with only one source node. A key contribution of this paper is an investigation of the effect that current drift has on networking. The performance of the routing protocols over time is measured, under a modified 3D Meandering Current Mobility model that takes into account lower current speeds with increased depth. Results show that even in a slow-moving coastal current, packet delivery in an initially dense network becomes unviable within 3 hours of drift. This work suggests controlled mobility management be investigated in future to extend network lifetime.

Categories and Subject Descriptors

C.2.2 [**Computer-Communication Networks**]: [Underwater Sensor Networks, Routing Protocols, Underwater Mobility]

General Terms

Performance, Mobility

Keywords

Underwater Sensor Networks, Meandering Current Mobility, Geographic Routing, Oil Spill Tracking

WUWNet'12, Nov. 5 - 6, 2012 Los Angeles, California, USA.

1. INTRODUCTION

An underwater acoustic sensor network (UASN) consists of a scalable ad-hoc network comprised of low-cost sensor nodes that transmit data over multihop routes to sink nodes using acoustic communications. UASNs are envisioned to be able to provide large-scale 4D real-time monitoring of the marine environment. Applications for UASNs include ocean sampling networks, pollution monitoring, undersea exploration such as to identify resources for commercial exploitation and tactical surveillance[1]. Fixed UASNs have been set up in which nodes are set in the seabed or attached to moorings or buoys[1][10]. Manually deploying nodes this way is more complicated and limits the scale of the network. Mobile nodes can instead be dropped in large numbers to provide continuous coverage, using a buoyancy-adjusting oil bladder system to dive to their required depth in the network and to surface for recovery and reuse[6]. The topology of a mobile 3D UASN is shown in Figure 1. As conventional radio frequency (RF) based wireless communications is only usable above the water's surface, data is transmitted across short-range acoustic broadcast links via multi-hop routes to sink nodes on the surface, which are equipped with long-range satellite or radio transceivers to deliver the data to a monitoring station.

While mobile UASNs have been proposed for both short-term time critical applications and long-term monitoring[6], it is unclear how long the network will remain connected and how the performance of the network will evolve under drift. In particular, the speed of underwater currents has

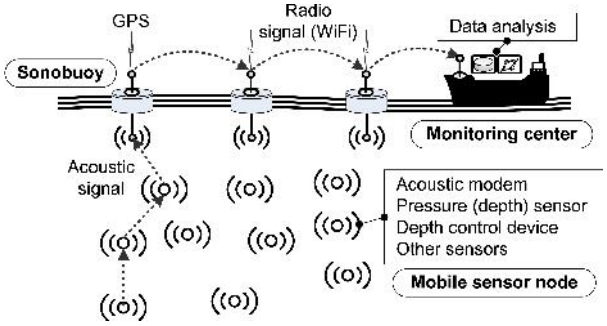

Figure 1: Mobile 3D underwater acoustic sensor network architecture[11]. Both underwater and surface nodes are untethered and drift with the water currents.

been measured to fall as depth increases[9], which suggests the network will tend to shear apart over time[1]. Routing protocols designed for such networks should consider the full lifetime of the deployment so that near optimal quality of service is provided when the network is initially dense and performance declines gracefully as nodes move apart.

This paper focuses on mobile UASNs consisting of untethered nodes and studies the impact current mobility has on network connectivity and the performance over time of two pressure routing protocols recently proposed for multiple-sink architecture mobile UASNs, viz., Depth Based Routing (DBR)[20] and HydroCast[11]. The protocols are evaluated in simulation where continuous sensed data, originating from the bottom network layer, needs to be delivered. Nodes drift under a realistic physically-inspired 3D mobility model – a modified version of the Meandering Current Mobility model (MCM) [5] for Lagrangian transport in coastal currents that is based off real-life observations of the Gulf Stream current. In this paper, we have extended the model to factor in maximum current speeds that vary with depth. While DBR and HydroCast have been previously compared, e.g. [11, 19], they have only considered random mobility[19] or depth-invariant mobility[11]. In addition, results have focused on the averaged performance over the entire simulation rather than the change in performance with time as the network drifts apart. This is the first attempt to study the routing of data from the bottom layer of the network to sinks on the surface. Our results show that the performance degrades significantly with time as the network becomes more dispersed.

This research is motivated by the 2010 *Deepwater Horizon* oil spill in the Gulf of Mexico. As well as being the largest offshore oil spill in history[4], the disaster was also the first of its type, a deep water blowout, resulting from an explosion at the wellhead causing oil to spill out at a depth of 1500 m. In the cleanup effort, dispersants were injected directly at the wellhead that produced large undersea plumes of suspended oil particles. A new phenomena, these plumes reaching over 35 km in length were discovered to drift in a Lagrangian fashion with the currents at a depth of 1000–1200 m[4]. At that time, observations of the plumes were made by ship-based rosette sampling, remotely operated underwater vehicles (ROVs) and autonomous underwater vehicles (AUVs)[4]. Such techniques are expensive and small-scale, with ships requiring a crew and a long voyage time while AUVs are deployed singly and results are not gathered back until some days later when the AUV finishes its mission. Significant enhancements are possible with mobile UASNs, which are envisioned to provide large-scale dynamic monitoring coverage with data reported back in real-time from the depth horizon where the oil plume is found.

The paper is organized as follows. In Section 2 underwater routing protocols are briefly discussed. The choice of routing protocols and the differences this performance study has with existing works are explained. Section 3 examines the mobility model used to simulate realistic drift in nodes. The scenario design and performance metrics are then defined in Section 4, where DBR and HydroCast are described in more detail. The simulation results are presented in Section 5 with a discussion. Finally, Section 6 concludes the paper with directions for future work.

2. RELATED WORK

A number of routing protocols have been developed over the past few years specifically for UASNs[11–13, 15, 18–20] that attempt to address the challenges presented by the harsh underwater channel. For a recent qualitative survey of UASN routing protocols, the reader is referred to [2, 7]. Most of the mobile UASN protocols being proposed use geographic routing[11, 13, 19, 20]. While geographic routing obviates the need for route request flooding and is scalable since decisions are made locally, full-dimensional node localization required by these protocols cannot always be guaranteed underwater. To overcome the lack of localization underwater, a variant known as pressure routing protocols[11, 13, 20] emerged. Sinks are located on the water's surface, and thus, packets are forwarded upwards using the local depth or pressure information of a node and its neighbors. Depth information can be easily obtained by providing each node with an inexpensive strain gauge-based pressure sensor. As long as a packet arrives at a sink, the packet is considered to be delivered to the monitoring center, since each sink is equipped with a long-range radio for direct communications[20]. Pressure routing assumes that sinks are sufficiently distributed so that the packet is received by at least one when it reaches the surface.

The first such pressure routing protocol is DBR[20] which includes, in the packet header, the depth of the sender in the current hop. Nodes decide to forward an overheard transmission if the difference in this value and the sensor's own internally measured depth exceeds a certain threshold. In this way nodes that provide only minimal advancement to the surface are able to ignore the packet. HydroCast[11] avoids a number of problems that occur in DBR. The primary difference is that the sender defines in the packet header a *forwarding set* of hidden-terminal free nodes that should attempt to forward the transmission, whereas in DBR the holding time cannot suppress transmissions from neighbors suffering from the *hidden terminal problem* where each node is within reception range of the previous hop but not each other. Most recently Void Aware Pressure Routing (VAPR) has been proposed in [13] and extends HydroCast by using geo-opportunistic directional data forwarding to avoid and route out of void areas. DBR and HydroCast will be further elaborated in subsections 4.2 and 4.3 respectively.

The treatment of underwater mobility has been relatively lacking in the literature. Routing protocol simulations have mainly used stochastic mobility models popular in ad-hoc network research to represent the movement of free-floating nodes, most often, random waypoint[20] mobility. Such processes are not appropriate for approximating current processes. Rather than being independent, the motion of nearby nodes is expected to be highly correlated as they are being advected by the same overall current velocity field. Nodes are also not confined to the initial box where they are deployed but will drift over large distances. Previous works using DBR have simulated the protocol in a static network[19] and under random waypoint mobility[20]. Recently, physically-inspired node mobility models have been proposed such as the MCM model[5]. HydroCast and DBR are simulated using this model in [11, 13]. However, the model employed does not consider changes in current with depth and the performance of the protocols over time are not discussed, which this paper covers.

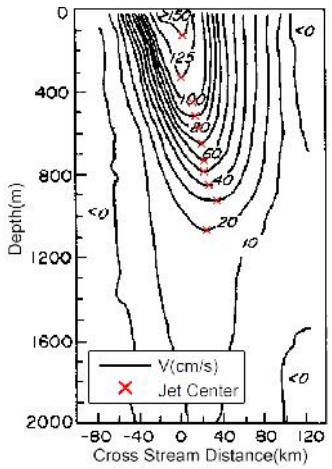

Figure 2: Average downstream velocity of the Gulf Stream at 73°W, based off measurements by Halkin and Rossby[9]

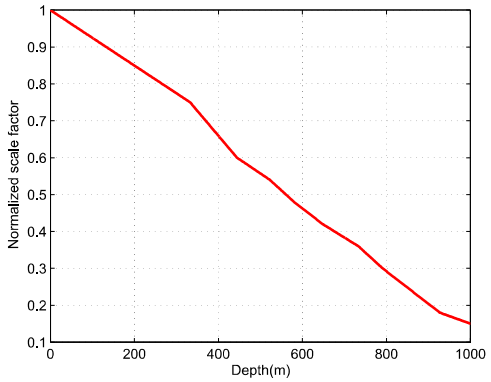

Figure 3: Mobility model scale factor $\psi_0(z)$, against depth, relative to the surface value

3. UNDERWATER MOBILITY MODEL

The MCM model[5] represents a meandering jet and is based off the streamfunction proposed in [3, 17] to describe the trajectories of fluid parcels in the Gulf Stream. The MCM model was originally proposed for 2D underwater networks as a realistic physically-inspired drift model and has since been employed in a number of simulations[8, 11, 13].The movement of nodes in the model is defined by the nondimensional streamfunction[5]

$$\psi(x,y,t) = 1 - \tanh\left(\frac{y - B(t)sin(k(x-ct))}{\sqrt{1+k^2B^2(t)cos^2(k(x-ct))}}\right) \quad (1)$$

where $B(t) = A + \epsilon\cos(\omega t)$ and a unit of time and distance is equal in physical units to $\psi_0^{-1}\lambda^2$ and λ[17]. The value λ determines the width of the jet and ψ_0 is referred to as the scale factor. The Cartesian sensor velocities (u', v') in the x (eastward) and y (northward) directions are obtained by computing $u' = -s_c\frac{\partial\psi}{\partial y}$ and $v' = s_c\frac{\partial\psi}{\partial x}$, with the terms being scaled back to real units by $s_c = \psi_0\lambda^{-1}$, the maximum speed in the center of the jet.

To model the realistic drift of untethered sensors in a 3D network in this paper's simulations, we extend the MCM model by incoporating changes in current velocity with depth. Extended 3D variants of the MCM model used in [8, 11, 13] simply advect nodes by the same 2D streamfunction projected to the depth the node resides on. The Meandering Current Mobility with Surface Effect (MCM-SE) model in [8] further introduces stochastic horizontal velocity perturbations that are superposed onto the MCM velocity field, if the depth is less than 250m, in order to represent the action of wind on the ocean. However the speed of currents is known to vary along the water column. In wind-driven currents the energy of the wind is transmitted to the lower layers by the turbulent mixing of fluid parcels. The proportion of energy transferred depends on how well the layers are stratified. If there is a sharp change in density, such as can occur at a thermocline, very little turbulent mixing can occur and minimal lower layer motion is produced[14].

The MCM streamfunction is developed in [3] to explain the different trajectories of RAFOS floats deployed at various depths. The scale factor ψ_0 is chosen to produce values for the maximum current speed s_c measured in the Gulf Stream[9] of $200kmd^{-1}$ on the surface and decreasing to $50kmd^{-1}$ at the lower thermocline. The model correctly predicts increased exchange between the jet with depth as seen in the float observations. Taking a cue from this approach, in this paper the value of ψ_0 is scaled with depth to model the real-world vertical variation in current speed.

The streamfunction is now given by:

$$\psi(x,y,z,t) = 1 - \tanh\left(\frac{y - B(t)sin(k(x - c\frac{\psi_0(z)}{\psi_0(0)}t))}{\sqrt{1+k^2B^2(t)cos^2(k(x-ct))}}\right) \quad (2)$$

The resulting equations for the dimensional x,y and z-velocity of nodes in the modified 3D MCM mobility model are:

$$u'(x,y,z,t) = -\psi_0(z)\lambda^{-1}\frac{\partial\psi(x,y,z,t)}{\partial y} \quad (3)$$

$$v'(x,y,z,t) = \psi_0(z)\lambda^{-1}\frac{\partial\psi(x,y,z,t)}{\partial x} \quad (4)$$

$$w'(x,y,z,t) = 0 \quad (5)$$

where $B(t) = A + \epsilon\cos(\omega t)$, the physical units for distance and time are nondimensionalized according to $d' = k_d d = \lambda d$ and $t' = k_t t = (\psi_0(0))^{-1}\lambda^2 t$. Time is nondimensionalized according to the speed at the surface reference level so the streamfunction must apply a correction factor $\psi_0(0)$ at different depths. Nodes only move horizontally in this model.

The downstream speed of the Gulf Stream plotted in [9] and reproduced here as Figure 2 is used to model a realistic dropoff in the current speed with depth. The scale factor $\psi_0(z) \propto s_c(z)$ is scaled in this paper according to Figure 3, which is obtained by fitting the values at the marked points of Figure 2. The resulting mobility model consists of a meandering jet. The pattern of meanders propagates to the east with phase speed $c' = \frac{k_d}{k_t}c$. The streamfunctions of the model, which has been configured as a typical coastal current[5], at depths of 0 m and 500 m are shown in Figure 4. The streamfunctions are depicted in the comoving frame, moving at phase speed, and represent the trajectory of nodes if the streamfunction did not change with time. The jet can be clearly seen. At the edge of the meander crests, nodes move eastwards slower than the phase speed and are left behind by the jet. The nodes do not continue along the jet until the next peak passes them. This gives rise to the appearance of recirculating vortices in the comoving frame,

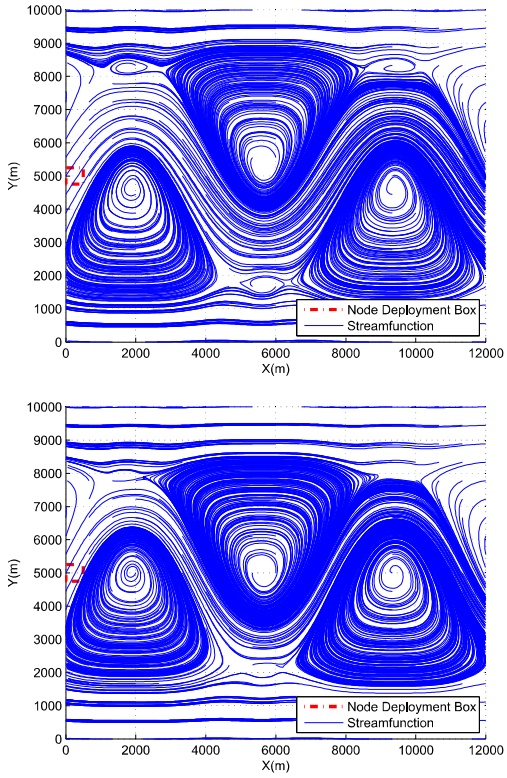

Figure 4: Mobility model streamfunction in the co-moving frame of reference at $t = 0$s at (a)depth= 0 m, $s_c = 0.39\,\mathrm{ms}^{-1}$ and (b)depth= 500 m, $s_c = 0.22\,\mathrm{ms}^{-1}$. Model parameters after a typical coastal current: $A = 1.2$, $c = 0.12$, $k = 2\pi/7.5$, $\omega = 0.4$, $\epsilon = 0.3$, where non-dimensional units are 1 km for space and 0.03 days for time.

the size of which are visibly larger at greater depths while the width of meanders are the same.

4. SIMULATION SETUP

The design of the simulation study is detailed in this section. DBR and HydroCast are presented in more detail, and where the original protocols have been modified for the simulations, these changes are highlighted.

4.1 Simulation Settings

The simulations are run on QualNet 5.0. The network setup is based on the original DBR validation simulation [20] with parts of the HydroCast simulation in [11], such that valid comparisons with these papers' results can still be made. The primary difference is that the number of sources along the bottom of the network is increased from just one in order to evaluate a realistic network application that is interested in sensed data occurring across the lowest layer, such as an oil plume.

Nodes are randomly deployed in a 500 m×500 m×500 m 3D space[20]. Ten sinks are randomly placed on the water's surface while ten sources are distributed at depth 500 m, with between $100 - 600$ other sensors making up the rest of the network. Sources transmit on average one 50 byte packet per second, before other headers are added, at 50 kbps[11]. The original DBR scenario data rate of 10 kbps led to too much congestion, where network capacity was having the most effect on the performance instead of the routing protocols. The size of the data packet with all headers included except the routing header is 94 bytes, as QualNet requires adding UDP and IP headers. Packets are generated at the source on each second but are not transmitted until after a short delay, uniformly randomly selected from lasting between 0 and 1 s, to prevent synchronization. At the link layer, a CSMA (carrier sense multiple access) MAC (media access control) protocol is used[20]. A packet is dropped if the number of backoffs exceeds four.

The physical layer in the DBR simulation is not clearly described. Only a transmission range of 100 m is stated, which presumes a binary erasure channel. In this paper, the more realistic channel model in [11] is adopted. The path loss is defined by the Urick propagation model, $A(d, f) = d^k a(f)^d$, where d is the distance, f is the signal frequency, the spreading factor $k = 1.5$ and Thorp's formula is substituted for the absorption coefficient $a(f)$. The underwater propagation speed is fixed at $1500\mathrm{ms}^{-1}$. Rayleigh fading is assumed and the bit error rate (BER) at the receiver is calculated for BPSK (binary phase shift keying) modulation at that signal-to-noise ratio (SNR). A packet is only successfully received if there are no bit errors. The transmit power is set to 105 dB re μPa and the receiver sensitivity and noise power to 75 dB so that with path loss the SNR of the signal is 0dB and just barely undetectable at a distance of 100 m, which is consistent with the transmission range of the LinkQuest UWM1000 commercial underwater acoustic modem. The power consumption of this model is used for sensors in this paper. In sending, receiving and idle modes nodes consume 2W,0.1W and 10mW of power respectively.

All nodes in the simulation move under the extended MCM mobility model defined in Section 3, with parameters chosen from [5] for typical coastal currents of $A = 1.2$, $c = 0.12$, $k = 2\pi/7.5$, $\omega = 0.4$, $\epsilon = 0.3$ and with non-dimensional units for time and distance of 0.03 days and 1 km. To account for the vertical current variation, the scale factor $\psi_0(z)$ in the mobility model equation is scaled by the fitted curve in Figure 3, where $s_c(0) = \frac{1km}{0.03d} = 0.39\,\mathrm{ms}^{-1}$. Streamfunctions for these settings are depicted in Figure 4. The box volume where nodes are initially deployed in the mobility model pattern is delineated in red. The position of nodes every 10 s is found by numerically integrating the velocity field from Equation (5) in MATLAB using a fourth-order Runge-Kutta method. The co-ordinates are fed into QualNet as waypoints and in simulation nodes move with constant speed to reach each new position just as the interval elapses.

The effect of mobility on the network topology is measured by the node connectivity. A node is connected if any multi-hop route exists to a sink, where the degree of connectivity is equal to the number of distinct sinks the node is able to reach. The main routing protocol performance metrics that are considered are packet delivery ratio (PDR), end-to-end delay and energy consumption. The PDR of a source is the proportion of packets received correctly by at least one sink over the total number of packets sent. The time between when a packet is sent until the earliest time it reaches a sink comprises the end-to-end delay, and only considers delivered packets. The total energy consumption of the network is

used to judge the overhead of the protocol.

The network was simulated over 3 hours under both DBR and HydroCast. Two types of simulations were run. In the first case the mobility model was processed offline to calculate the distribution of nodes at each half-hourly interval $t = \{0.0, 0.5,\ 1.0, 1.5, 2.0, 2.5, 3.0\}$ h and their motion 200 s either side of this time. The simulation was then executed. The network was left to run for the first 200 s, with statistics only being gathered during the latter 200 s once the network has stabilized. This provides a discrete snapshot of the PDR and end-to-end delay at the corresponding point in the network's drift. The scenario was run over the full 3 hour duration in the second type to record the overall energy consumption. The network was simulated with $n = 100 - 600$ sensors in 100 increments. Not all network sizes are plotted later on for clarity. Each simulation is repeated 20 times with different seeds used to generate the initial $t = 0$ s randomly deployed node distributions. These seed values have been kept consistent between the full and discrete simulations and runs testing different network parameters, so the topology statistics at a particular time over one set of 20 runs is the same across all simulations. No seeds are needed for the modified MCM mobility model, which is deterministic. The median value of 20 runs are reported with uncertainty bars consisting of the 25% and 75% quartiles of measured results.

4.2 Depth-Based Routing

DBR is tunable using two parameters, the depth threshold d_{th} and the holding time parameter δ. In DBR, packets are routed exclusively using a greedy forwarding algorithm. Nodes that overhear a transmission decide to forward it if the difference between the depth of the packet's previous hop d_p and the current node d_c exceeds the depth threshold, that is $d_{th} \leq d_p - d_c$. Nodes wait a linear holding time:

$$T_{\mathrm{H}} = \alpha(R - (d_p - d_c))) \tag{6}$$

before forwarding the packet, where the coefficient $\alpha = \frac{2R}{v_0}\delta$. R is the maximal transmission range of the sensor and v_0 is the speed of sound underwater, which are set for DBR to 100 m and 1500 ms^{-1} in the simulation. The holding time varies inversely linearly with $d_p - d_c$, causing higher nodes closer to the sinks to forward the packet first. Lower waiting nodes that hear the following broadcast are able to cancel their now redundant transmission. If queueing and processing delays are negligible as well as the transmission duration of the packet, then the packet first broadcast by node i will be received in time by lower node j to cancel its own transmission if $d_i - d_j \geq \delta$ [20]. A smaller value of δ can prevent more redundant broadcasts but at the expense of longer holding times. When the packet transmission delay is included, the broadcast is received in its entirety in time to prevent the lower node from sending if

$$\alpha > \frac{t_{ci} - t_{cj} + t_{ij} + t_{data}}{d_i - d_j} \tag{7}$$

where t_{ab} is the propagation delay from node a to node b and t_{data} is the transmission delay of the data packet. The DBR data packet header is 16 bytes long as simulated in this paper and the total size of the data packet at the physical layer is 110 bytes.

4.3 HydroCast

A major problem with DBR is that the depth threshold and holding time parameter are fixed during the operation of the protocol. HydroCast in effect leverages neighbor information to find the optimal holding time and forwarders at each hop. Beacons are periodically broadcast for nodes to acquire information on neighbor depths and distances to their two-hop neighbors. A heuristic algorithm finds a cluster of hidden terminal-free nodes lying above the node that, out of all its neighbors, would maximize the expected depth-wise advance to the surface if a packet was forwarded to them. When the node has a packet to send, it is able to specify these nodes in the packet header. Only the nodes in this *forwarding set* will attempt to forward the packet.

Like DBR, forwarders wait a linear holding time given by Equation (6) before transmitting. As the forwarders and their pairwise distances are known in HydroCast, the value of the holding time coefficient α is adaptively set to the minimum value in Equation (7). Ideally, if any node in the cluster forwards the packet, all other redundant transmissions are suppressed as other holding cluster members are able to overhear the broadcast in time and there are no hidden terminals. In comparison the static holding time parameter value, δ, in DBR cannot guarantee redundant transmissions are prevented if the separation between nodes is smaller, or causes an excess delay to be waited.

In greedy forwarding, a problem may arise when the node is in a *void area* where there are no neighbors that move the packet closer to the destination. In DBR, the protocol reaches a dead-end. However, HydroCast specifies a local lower-depth-first recovery mode where nodes that are local maxima are required to maintain a route along the void floor surface of the network to another node of lesser depth, so that packets can be routed out of the void area and greedy forwarding can be resumed at this point. Both local maxima and surface status can be obtained from beacon neighbor status. Details of the recovery mechanism are not available in [11].

HydroCast is configured with the same parameters in this paper's simulations as those reported in [11]. Beacons are exchanged every 30 seconds plus a jitter that is interpreted here as an additional delay uniformly randomly selected between $0 - 30$ seconds. The beacon data is set to expire after 90 seconds if not updated by the same neighbor. Parameter k -the number of random vectors checked for domination to determine whether the node is on the network face- is set to 20 and a Bloom filter of size 150 bits is used to store the forwarding set. The variable $\beta = 0.5$ and the maximum allowable delay per hop $\gamma = 1.0$ s/m.

HydroCast is evaluated with and without the recovery mechanism in this paper, labelled as HydroCast-RECOVERY and HydroCast-GREEDY respectively. With lower-depth-first recovery, packets that end up in a local maxima are flooded by nodes on the void floor surface until a higher sensor is reached and switches back to greedy forwarding. Nodes that receive a flooded packet do not wait a holding time as the forwarding set is not known to adaptively set α. The sizes of the flooding and data packets at the physical layer in QualNet are 126 bytes and 161 bytes. The beacon size varies with the number of neighbors. The maximum size observed was 204 bytes.

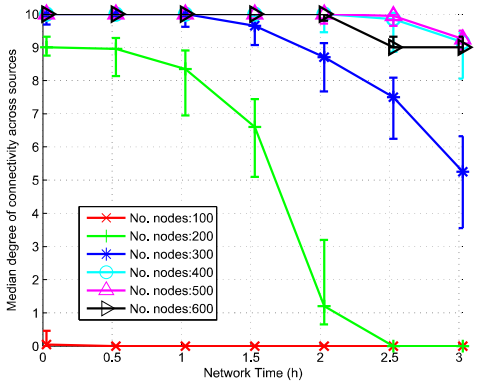

Figure 5: Median degree of ideal connectivity across sources under different network sizes, against time

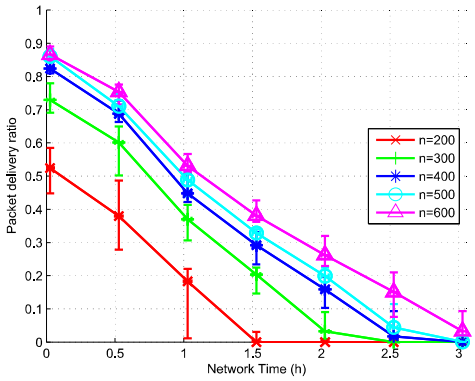

Figure 6: Median packet delivery ratio of DBR under different network sizes; $\delta = 100\,\text{m}$, $d_{th} = 0\,\text{m}$

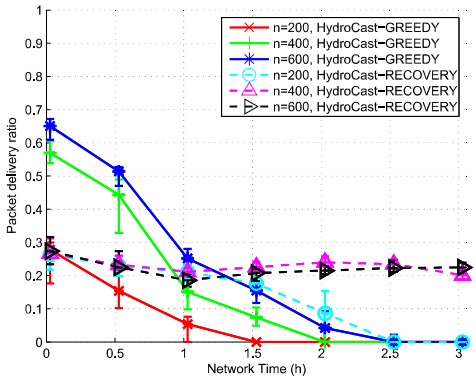

Figure 7: Median packet delivery ratio of HydroCast with lower-depth-first recovery flooding disabled and enabled under different network sizes.

5. PERFORMANCE RESULTS

In this section, we discuss the performance based on four metrics: degree of connectivity, PDR, end-to-end delay and energy consumption.

Degree of connectivity: Results shown in Figure 5 are obtained by analyzing the node positions at each half hour. Devices are considered to be in communications range if they are within $100m$ of each other in any direction, and a brute force search along all hops is performed to determine how many sinks each source could reach. The results show sources lose contact through the network to the sinks on the surface with time, which is expected. The maximum speed of nodes in the center of mobility model jet decreases with depth, from 0.39ms^{-1} on the surface to $0.22\,\text{ms}^{-1}$ at 500 m depth where the sinks are sequestered. Not only that but, as shown in Figure 4, when this speed is lower the region of recirculating vortices extends deeper towards the center of the meandering jet. At the surface the initial deployment area is squarely in the meandering jet. However, at 500 m depth, the bottom right corner is grazing the edge of a vortex, where it is detrained from the jet and not picked up until the next crest passes over it, which ultimately causes nodes located at this depth to not progress as fast downstream in the jet. After $t = 1.5\,\text{h}$, sources are completely disconnected in the 100-node network and this network size is omitted from later figures as the scenario does not produce any meaningful results. Only the 200- and 300-node topologies display a large decrease in the degree of connectivity between $t = 0 - 3\,\text{h}$. For $n = 400 - 600$, sources are still connected to a median of at least 8 out of a possible 10 sink nodes after $t = 3\,\text{h}$.

PDR: Unlike the connectivity, a proportionate change is not reflected in the PDR performances of both protocols, which are plotted separately in Figures 6 and 7. A general choice of parameters for DBR is used where $d_{th} = 0\,\text{m}$ and $\delta = 100\,\text{m}$, the maximal transmission range, which is found in [20] to give the best end-to-end delay with negligible increase in energy consumption. In the cases of both DBR and HydroCast-GREEDY, the PDR has declined to zero or near-zero within time $t = 3\,\text{h}$ of the network being deployed. The PDR increases with the number of nodes deployed, although the benefit becomes minor above 400 nodes where boosting the network size to 600 nodes, a 33% increase, only changes the initial PDR of DBR by 5%. However, even with 600 nodes, the PDR of the network when DBR is used at $t = 3\,\text{h}$ is 3.3% compared to 87% at $t = 0\,\text{h}$. Nodes do not fail or run out of energy in the scenario, so this dropoff is entirely due to mobility. The performance over time of HydroCast-RECOVERY is completely different. An 18% dropoff in PDR between $t = 0\,\text{h}$ and $3\,\text{h}$ is measured for the network sizes $n = 400$ and 600 nodes that is consistent with the change in connectivity degree observed in Figure 5, which decreases from 10 to more than 8 sink nodes. This indicates that sufficient routes to the surface still exist that can be followed by downward flooding around void areas, but which DBR and HydroCast are prevented from exploiting if only greedy forwarding to upper nodes is allowed.

The PDR of HydroCast-GREEDY is lower than DBR and follows a similar falloff trend with time. On average, the PDR is 53% less at $t = 0\,\text{h}$. The PDR of HydroCast is also worse than DBR in [11], but, in their results, enabling lower-depth-first recovery leads to HydroCast outperforming DBR. Here, the PDR of HydroCast-RECOVERY is initially identical to within uncertainties with network size but has less than half the value of DBR or HydroCast-GREEDY. The face routing protocol used by [11] is not specified. Surface flooding and route discovery packets are both mentioned. It may be that paths are stored in [11], whereas in this implementation the packet is always flooded that results in more channel contention and dropped packets. The scenarios are also different. The parameters used for DBR are also not defined in [11] and a fixed holding time is em-

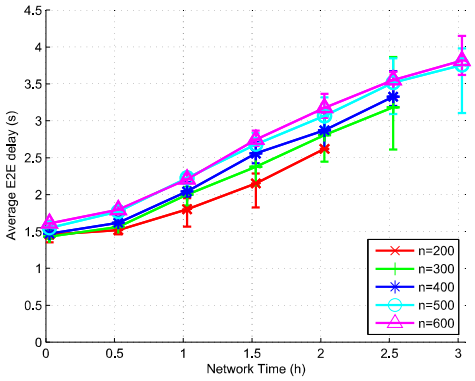

Figure 8: Median end-to-end delay of DBR under different network sizes; $\delta = 100\,\text{m}$, $d_{th} = 0\,\text{m}$

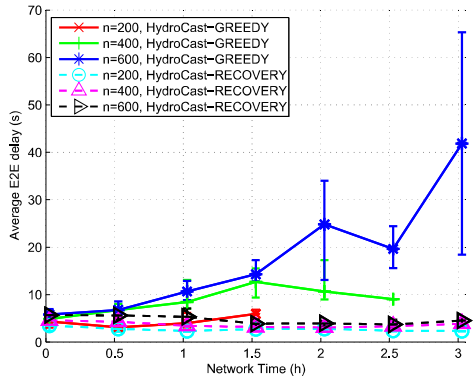

Figure 9: Median end-to-end delay of HydroCast with lower-depth-first recovery flooding disabled and enabled under different network sizes.

ployed, whereas [20] specifies a linear holding time.

Delay: The end-to-end delay over 200 s with the network at different time states is plotted for DBR in Figure 8. The latency at $t = 0\,\text{h}$ is virtually identical for different network sizes, which matches the results in [20]. As the network drifts apart with time, the delay increases. This is attributed to packets having to travel laterally over a greater total distance to sinks that have moved further ahead in the jet. Lines terminate before $t = 3\,\text{h}$ when no packets are received by any sinks to calculate the latency. Figure 9 shows the end-to-end delay for HydroCast. The latency for HydroCast-GREEDY is higher than HydroCast-RECOVERY, but shows no consistent upwards or downwards trend with time. Greedy forwarding causes nodes to wait an adaptive holding time. With face routing, packets are also flooded that are immediately sent to the MAC layer for transmission. The maximum holding time can be set by varying γ and, in future work, it would be worthwhile to investigate the effect this parameter has on end-to-end delay, packet delivery ratio and energy consumption in HydroCast. The large uncertainty bars observed as time increases arise when the existence of routes is highly dependent on the distribution of nodes in a sparse network. The static end-to-end delay over time of HydroCast with lower-depth-first recovery suggests that the increasing lateral separation of sinks and sources under drift and the lengthening of the propagation time is being balanced.

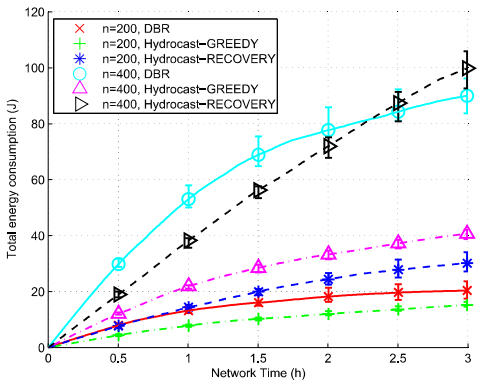

Figure 10: Median total network energy consumption for DBR and HydroCast, where the number of nodes $n = 200$ and 400. DBR: $\delta = 100\,\text{m}$, $d_{th} = 0\,\text{m}$

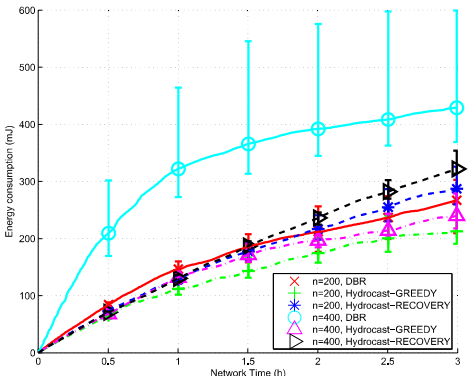

Figure 11: Maximum individual node energy consumption for DBR and HydroCast, evaluated out of all sensors in the network, where the number of nodes $n = 200$ and 400. The median energy across simulation runs is plotted. DBR: $\delta = 100\,\text{m}$, $d_{th} = 0\,\text{m}$

Energy consumption: Energy management underwater is crucial. Not only does acoustic communications requires more power than terrestrial RF signals but UASNs are less densely deployed than land-based WSNs, and therefore less tolerant to the loss of links. Two types of energy graphs are plotted using the running results from the full 3 hour network simulations. The total network energy consumption summed across all devices is plotted in Figure 10 for $n = 200$ and 400 sensors. As expected, the larger and hence denser network has higher absolute energy consumption as there are more receivers per hop and redundant forwarders.

The maximum energy consumption by any sensor in the network up to this point in time is graphed in Figure 11. The intersection of any curve with the sensor battery capacity allows the lifetime of the network to be determined, which can be defined as the time until the first node runs out of energy[16]. The results show that the additional forwarder suppression of HydroCast-GREEDY produced by a hidden terminal free forwarding set and adaptive holding time reduces the network energy consumption of the protocol below DBR, despite extra header and beacon overhead. Adding 2D surface flooding causes HydroCast-RECOVERY's energy

consumption to exceed DBR and the rate of consumption does not decrease as fast as other protocols with time but remains almost constant. This matches its largely static end-to-end delay and PDR. However, measuring energy consumption by the maximum sensor usage shows that the network has the shortest lifetime under DBR.

6. CONCLUSION

The impact current mobility has on underwater acoustic sensor networks is a major issue. In this paper, the performance of two pressure routing protocols: DBR and HydroCast is evaluated in a simulated UASN drifting under a physically-inspired mobility model, which has been configured to model 3D coastal currents. Data is generated along the bottom network layer, like in submarine or oil plume monitoring applications. During the *Deepwater Horizon* oil spill, a concern was being able to track undersea oil plumes if they became entrained in the fast-flowing Loop Current. The results show that void recovery in geographic routing protocols allows the protocol to still operate after the network has drifted over a longer period. The packet delivery ratio of HydroCast only decreases by 18% after 3 hours, whereas DBR, which only uses greedy forwarding, cannot route any packets to sinks. Controlled node mobility could be used to reduce the proportion of local depth minimum nodes and void areas, which increases as the network becomes sparser. Development of a distributed topology reorganization scheme that adjusts the depths of nodes is planned for future work.

7. REFERENCES

[1] I. Akyildiz, D. Pompili, and T. Melodia. Underwater acoustic sensor networks: research challenges. *Ad hoc networks*, 3(3):257–279, May 2005.

[2] Y. Bayrakdar, N. Meratnia, and A. Kantarci. A comparative view of routing protocols for underwater wireless sensor networks. In *OCEANS, 2011 IEEE-Spain*, pages 1–5. IEEE, 2011.

[3] A. Bower. A simple kinematic mechanism for mixing fluid parcels across a meandering jet. *Journal of Physical Oceanography*, 1991.

[4] R. Camilli et al. Tracking hydrocarbon plume transport and biodegradation at Deepwater Horizon. *Science*, 330(6001):201–4, Oct. 2010.

[5] A. Caruso et al. The Meandering Current Mobility Model and its Impact on Underwater Mobile Sensor Networks. In *Proceedings of IEEE INFOCOM*, pages 221–225, Apr. 2008.

[6] J. Cui, J. Kong, and M. Gerla. The challenges of building mobile underwater wireless networks for aquatic applications. *IEEE Network*, 20(3):12–18, 2006.

[7] K. Dongkyun and A. Wahid. Analyzing Routing Protocols for Underwater Wireless Sensor Networks. *International Journal of Communication Networks and Information Security (IJCNIS)*, 2(3):253–261, 2011.

[8] M. Erol et al. Multi Stage Underwater Sensor Localization Using Mobile Beacons. *2nd International Conference on Sensor Technologies and Applications (SensorComm 2008)*, pages 710–714, 2008.

[9] D. Halkin. The structure and transport of the Gulf Stream at 73 W. *J. Physical Oceanography*, 1985.

[10] M. Jiang. OceanSense: A practical wireless sensor network on the surface of the sea. *IEEE International Conference on Pervasive Computing and Communications*, pages 1–5, Mar. 2009.

[11] U. Lee et al. Pressure Routing for Underwater Sensor Networks. *IEEE INFOCOM*, pages 1–9, Mar. 2010.

[12] U. Lee, J. Kong, M. Gerla, J. Park, and E. Magistretti. Time-critical underwater sensor diffusion with no proactive exchanges and negligible reactive floods. *Ad Hoc Networks*, 5(6):943–958, Aug. 2007.

[13] Y. Noh, U. Lee, P. Wang, and B. Choi. VAPR: Void Aware Pressure Routing for Underwater Sensor Networks. *IEEE Transactions on Mobile Computing*, pages 1–14, 2012.

[14] Open University. *Ocean Circulation, Second Edition*. Butterworth-Heinemann, 2 edition, Aug. 2001.

[15] D. Pompili, T. Melodia, and I. Akyildiz. Distributed routing algorithms for underwater acoustic sensor networks. *Wireless Communications, IEEE Transactions on*, 9(9):2934–2944, 2010.

[16] R. Rajagopalan and P. Varshney. Data-aggregation techniques in sensor networks: a survey. *IEEE Comms. Surveys & Tutorials*, 8(4):48–63, 2006.

[17] R. Samelson. Fluid exchange across a meandering jet. *Journal of physical oceanography*, 1992.

[18] W. K. G. Seah and H.-X. Tan. Multipath Virtual Sink Architecture for Underwater Sensor Networks. *OCEANS 2006 - Asia Pacific*, pages 1–6, May 2006.

[19] A. Wahid, S. Lee, and D. Kim. An energy-efficient routing protocol for UWSNs using physical distance and residual energy. In *OCEANS, 2011 IEEE-Spain*, pages 1–6. IEEE, 2011.

[20] H. Yan and Z. Shi. DBR: depth-based routing for underwater sensor networks. *Ad Hoc and Sensor Networks, Wireless Networks,*, pages 72–86, 2008.